Influence of chemistry on the steady solutions of hydrogen gaseous detonations with friction losses

Fernando Veiga-Lopez, Luiz Maltez Faria, J. Melguizo-Gavilanes

Influence of chemistry on the steady solutions of hydrogen gaseous detonations with friction losses

Fernando Veiga-López[a,*], Luiz M. Faria[b], Josué Melguizo-Gavilanes[a]

[a] *Institute Pprime, UPR 3346 CNRS, ISAE-ENSMA, 86961, Futuroscope-Chasseneuil, France*
[b] *POEMS, CNRS-INRIA-ENSTA Paris, Institut Polytechnique de Paris, Palaiseau, France*

Abstract

The problem of the steady propagation of detonation waves with friction losses is revisited including detailed kinetics. The derived formulation is used to study the influence of chemical modeling on the steady solutions and reaction zone structures obtained for stoichiometric hydrogen-oxygen. Detonation velocity - friction coefficient ($D - c_f$) curves, pressure, temperature, Mach number, thermicity and species profiles are used for that purpose. Results show that both simplified kinetic schemes considered (i.e., one-step and three-step chain-branching), fitted using standard methodologies, failed to quantitatively capture the critical c_f values obtained with detailed kinetics; moreover one-step Arrhenius chemistry also exhibits qualitative differences for $D/D_{CJ} \leq 0.55$ due to an overestimation of the chemical time in this regime. An alternative fitting methodology for simplified kinetics is proposed using detailed chemistry $D - c_f$ curves as a target rather than constant volume delay times and ideal Zel'dovich-von Neumann-Döring profiles; this method is in principle more representative to study non-ideal detonation propagation. The sensitivity of the predicted critical c_f value, $c_{f,\mathrm{crit}}$, to the detailed mechanisms routinely used to model hydrogen oxidation was also assessed; significant differences were found, mainly driven by the consumption/creation rate of the HO_2 radical pool at low postshock temperature.

Keywords: hydrogen, detonation, friction, chemical mechanisms.

*Corresponding author
Email address: fernando.veiga-lopez@ensma.fr (Fernando Veiga-López)

1. Introduction

In the upcoming global energy transition, hydrogen (H_2) has positioned itself as a promising fuel for several stationary and mobile energy conversion systems, such as fuel cells or direct combustion applications. Chemical reactions between pure H_2 and oxygen (O_2) release large amounts of energy and do not produce any CO_2, making H_2 very attractive to decarbonize industrial sectors such as long-haul transport, chemicals, and iron and steel production, where it is proving difficult to reduce emissions considerably [1]. However, there are still issues that need to be overcome before widespread use of H_2 becomes a reality [2]. The most pressing include: (i) the small size of molecular H_2 which makes it very prone to leaks in comparison to more conventional fuels (e.g., propane or natural gas); (ii) its low ignition energy and wide flammability limits which increase the risk of accidental combustion events; (iii) its low energy density which favors storage at very high pressures (70 MPa) to make it competitive/attractive for transport applications but increases the risk of unintended releases and explosion.

For instance, in the case of a fuel leak, very small concentrations of H_2 in air/O_2 are required to produce flammable layers which results in an increased likelihood of accidental ignition thereby posing a serious safety hazard. Such leaks usually occur in confined obstacle-laden geometries where upon ignition, and even without obstacles, accidentally-ignited flames may accelerate and potentially transition to detonation [3, 4]; a much more destructive combustion mode that may cause significant structural damage.

Gaseous detonations propagating in tubes are always subject to dissipation mechanisms, such as momentum, heat and curvature losses. Their steady structure and dynamics differ considerably from the more commonly studied ideal case. In this manuscript, we restrict our attention to the influence of momentum losses (i.e., friction) on one-dimensional detonations. Firstly addressed by Zeldovich [5] and revisited by many other researchers in subsequent works [6–11], it continues to be a relevant and an interesting problem in deto-

nation theory. From a practical point of view, accounting for losses is important to predict detonation propagation limits in tubes. Despite the rather strong simplifications typically required to develop a theory and/or low-order models, this approach should in principle provide reasonable and inexpensive predictions on whether or not a detonation can propagate given appropriate initial and boundary conditions. Thereby, anticipating the operating envelopes of systems powered by any reactive mixture and, in particular, by H_2. While we recognize that detonations are inherently unsteady and multidimensional, the propagation limits predicted by the proposed model may yield faster and conservative [12] estimates that are relevant for engineering risk assessment, which allow to cover a larger region of the parameter space at a fraction of the cost of running detailed transient two-dimensional simulations. The latter statement is supported by previous work using transient one-dimensional simulations with simplified kinetics and friction losses [12] which result in earlier failure than a quasi-steady model predicts (i.e., larger cross-sections/tube diameters for failure); current work in our group suggests a similar trend for detailed thermochemistry.

At any rate, it is known that friction plays two interesting roles on the physics of detonations: it simultaneously acts as a sink of momentum and a heat source. The former makes steady detonations subject to friction propagate at velocities lower than the ideal Chapman-Jouguet (CJ) value, D_{CJ}, whereas the latter is the sustaining mechanism at large velocity deficits –mixture dependent– ($D/D_{CJ} \leq 0.56$ for H_2-O_2), that is to say, when weak shocks are present. In such scenarios, the thermodynamic jump induced is not strong enough to trigger chemical reactions immediately behind the leading shock, and heating due to friction appears as a necessary mechanism for these self-sustained detonations to survive. At low post-shock temperatures, the aforementioned heating may become even more important than the exothermic chemistry itself.

Both physical effects are important on the two regimes that a detonation experiences when friction losses are included (see Fig. 1). On the one hand, for small velocity deficits

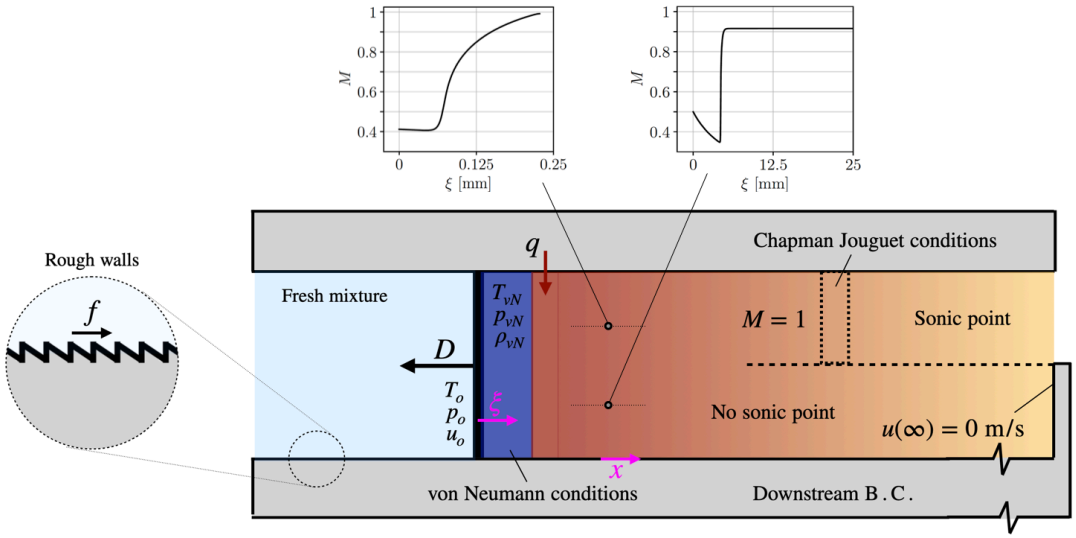

Figure 1: Schematic of a detonation propagating steadily at velocity D from right to left in a rough tube. The two possible solutions admitted by the governing equations are depicted (i) with a sonic point; (ii) without a sonic point. Note the stark differences in the length of the reaction zones.

($D/D_{CJ} \geq 0.56$) the wave structure is similar to a Zel'dovich-von Neumann-Döring (ZND) profile except that the presence of friction losses results in a slight temperature/pressure increase and associated density/velocity decrease before chemical reactions are activated. Under these conditions, a sonic point exists somewhere downstream the shock. On the other hand, for large velocity deficits ($D/D_{CJ} \leq 0.56$) the sonic point ceases to exist. In such cases, the wave structure resembles that of over-driven detonations supported by a piston [13]. In the absence of a sonic point the wave/reaction zone is affected by the downstream boundary condition which renders their structure significantly different from classical ZND detonations. However, the combination of chemical heat release and heating due to friction seems to be enough to sustain their propagation.

Most previous work on detonation propagation with friction losses, steady or unsteady, have considered the simplest description of the chemistry available [10–12, 14–20], i.e., one-step Arrhenius kinetics, which is thought to provide good qualitative agreement with real detonations [11], in addition to being particularly well-suited for theoretical studies. Simplified kinetic schemes, however, have recently been shown to perform poorly when quantitative

agreement is sought [21]. To our knowledge, only the work of Agafonov and Frolov [22], and that of Kitano et al. [23] and Suboi et al. [24] made use of detailed kinetics. The authors computed the minimum tube diameter for detonation propagation using a semi-empirical friction coefficient derived from Blasius boundary layer theory, and compared their results with experimental data; reasonable predictions were obtained. We note that in these articles, the authors restricted their attention to the critical diameters and not to an in-depth analysis of all the possible propagation regimes given by the locus of steady-states in $D - c_f$ space, nor to the reaction zone structures that appear at sub-CJ conditions. The objective of this paper is thus two-fold: (i) to assess the effect of chemistry modeling on $D - c_f$ curves and on the reaction zone structure of steady detonations with friction losses; (ii) to determine/quantify the detailed kinetics induced uncertainties on the predicted critical friction factors, $c_{f,\mathrm{crit}}$. To the best of our knowledge, no previous studies have addresses these issues.

The paper is structured as follows. Section 2 introduces a general mathematical formulation used to compute detonation waves with friction losses and detailed chemistry. The different chemical modeling and numerical method used are described in Section 3. Section 4 discusses the main results of our study via $D - c_f$ curves and spatial profiles of pressure, temperature, flow Mach number, thermicity and species mass fractions; an alternative fitting methodology for simplified kinetics using the $D - c_f$ curve obtained with detailed chemistry as a target is also described. Closing remarks are given in Section 5.

2. Mathematical formulation

2.1. Conservation form

One-dimensional detonations with friction losses [13] in tubes (sketched in Fig. 1) can be generally represented by the reactive Euler equations with a sink term in the momentum equation (2); a generic loss function of the form $f = P/(2A\phi)\tilde{c}_f\ \rho|u|u = c_f\rho|u|u$ where P represents the perimeter of the tube, A its cross-sectional area, ϕ its porosity and $\tilde{c}_f$ denotes

a dimensionless skin-friction coefficient of the rough walls of the channel. For a tube of circular cross-section and diameter, d, or a channel of square cross-section and side, L, this quotient P/A yields $4/d$ and $4/L$, respectively. In a generic way, we may obtain *a priori* the friction coefficient $c_f = P/(2A\phi)\tilde{c}_f$ with units m^{-1}, and later look for the dimensionless friction coefficient of a tube given its characteristics. Note that we perform a very simple approach for the porosity, considering a direct proportionality with the wetted area P/A with ϕ [11].

The system of equations reads:

$$\frac{\partial \rho}{\partial t} + \frac{\partial \rho u}{\partial x} = 0, \tag{1}$$

$$\frac{\partial \rho u}{\partial t} + \frac{\partial}{\partial x}\left[\rho u^2 + p\right] = -f, \tag{2}$$

$$\frac{\partial}{\partial t}\rho\left[e + \frac{|u^2|}{2}\right] + \frac{\partial}{\partial x}\rho u\left[h + \frac{|u^2|}{2}\right] = 0, \tag{3}$$

$$\frac{\partial \rho Y_k}{\partial t} + \frac{\partial \rho u Y_k}{\partial x} = W_k \dot{\omega}_k, \quad k = 1, ..., N, \tag{4}$$

where, ρ, u, p, e, h, x and t are the mixture density, axial velocity in the laboratory frame, pressure, specific internal energy, enthalpy (including the chemical contribution), and the spatial coordinate and time, respectively. The mass fraction, molecular weight and net production/consumption rate per unit mass of species k are given by Y_k, W_k and $\dot{\omega}_k$. Next, equations (1) - (4) are expressed in terms of the thermicity parameter $\dot{\sigma}$ which is a more convenient form for the sought after numerical solutions [25].

2.2. Thermicity form

After some rather tedious algebra, shown in Appendix A for completeness, the system becomes:

$$\frac{D\rho}{Dt} + \rho\frac{\partial u}{\partial x} = 0, \tag{5}$$

$$\rho\frac{Du}{Dt} + \frac{\partial p}{\partial x} = -f, \tag{6}$$

$$\frac{Dp}{Dt} - a_f^2\frac{D\rho}{Dt} = (\gamma - 1)uf + \rho a_f^2\dot{\sigma}. \tag{7}$$

$$\frac{DY_k}{Dt} = \frac{W_k\dot{\omega}_k}{\rho}, \quad k = 1, ..., N, \tag{8}$$

where the material derivative, D/Dt, the frozen speed of sound, a_f, and the thermicity parameter, $\dot{\sigma}$, are used for a more compact notation:

$$\begin{aligned} \frac{D}{Dt} = \frac{\partial}{\partial t} + u\frac{\partial}{\partial x}; \quad a_f^2 = \left.\frac{\partial p}{\partial \rho}\right|_{s,\mathbf{Y}}; \\ \dot{\sigma} = \sum_{k=1}^{N}\left(\frac{\overline{W}}{W_k} - \frac{h_k}{c_pT}\right)\frac{DY_k}{Dt}. \end{aligned} \tag{9}$$

The system above is closed with the ideal equation of state:

$$p = \rho\frac{R_u}{\overline{W}}T; \quad \overline{W} = 1/\sum_{k=1}^{N}(Y_k/W_k) \tag{10}$$

with R_u the universal gas constant and T and $\overline{W}$ the temperature and average molecular weight of the mixture.

2.3. Wave-fixed frame of reference / steady structure

For a frame of reference moving at a constant speed, $-D$, (i.e., the shock travels from right to left), unknown *a priori* and to be determined as a solution of a nonlinear eigenvalue problem, the following two variables are introduced, $\xi = x_s - x$ and w $= D - u$, which

represent a new spatial coordinate and velocity measured relative to the shock location, x_s, and wave speed, D, respectively. Substituting in the material derivative and seeking steady solutions only (i.e., $\partial/\partial t = 0$) the mapping is $D/Dt \rightarrow \mathrm{w}\mathrm{d}/\mathrm{d}\xi$. Furthermore, noting that $\mathrm{w} = \mathrm{d}\xi/\mathrm{d}t$, the system of equations reads,

$$\frac{\mathrm{d}\rho}{\mathrm{d}t} = -\rho\left[\frac{\dot{\sigma} + F_q + (\eta-1)F}{\eta}\right], \tag{11}$$

$$\frac{\mathrm{d}\mathrm{w}}{\mathrm{d}t} = \mathrm{w}\frac{\dot{\sigma} + F_q + (\eta-1)F}{\eta}, \tag{12}$$

$$\frac{\mathrm{d}p}{\mathrm{d}t} = -\rho\mathrm{w}^2\left[\frac{\dot{\sigma} + F_q - F}{\eta}\right], \tag{13}$$

$$\frac{\mathrm{d}\xi}{\mathrm{d}t} = \mathrm{w}, \tag{14}$$

$$\frac{\mathrm{d}Y_k}{\mathrm{d}t} = \frac{W_k\dot{\omega}_k}{\rho}, \quad k = 1, ..., N, \tag{15}$$

In Eqns. (11) to (15), $\eta = 1 - M^2$ is the sonic parameter and $M = \mathrm{w}/a_f$ is the Mach number relative to the leading shock computed using the frozen speed of sound, a_f. The main advantage of expressing the system using time, t, as the independent variable is that it simplifies the implementation in the Shock and Detonation Toolbox (SDT) [25]. The functions F_q and F are given by:

$$\begin{aligned} F_q &= \frac{(\gamma-1)}{a_f^2}c_f(D-\mathrm{w})^2|D-\mathrm{w}|; \\ F &= c_f\left(\frac{D}{\mathrm{w}} - 1\right)|D-\mathrm{w}|, \end{aligned} \tag{16}$$

where $\gamma = c_p/c_v$ is the ratio of the specific heats. It can be readily shown that for $c_f = 0$ m^{-1}, $F_q = F = 0$ which reverts the formulation to the ideal case included in Browne et al. [25]. The only changes required in the are thus adding the functions F_q and F, making it rather straight forward, and most importantly, allowing us to investigate arbitrary chemical mechanisms written in Cantera format [26] (i.e., *.cti* files); the complete derivation

is included in Appendix A.

The system of ordinary differential equations (ODEs) obtained is a two-point boundary value problem (BVP); the boundary condition at the shock ($t = 0$ s or $\xi = 0$ m) is computed using the shock jump conditions at a fixed initial pressure, temperature and composition, known as the von Neumann (vN) state. The boundary condition downstream depends on the nature of the problem. There are two possibilities: solutions with/without sonic points downstream. This is discussed at length in the following sections.

2.4. Chemistry modeling

One of the most important steps of this study is the choice made to model the interaction between the chemical heat release and the gas dynamics. Next, we describe the different approaches used to subsequently analyze its influence on the steady solutions admitted by the system of ODEs just derived.

2.4.1. 1-step chemistry

The simplest approach is to consider that reactants are directly converted into products via one irreversible reaction, and model its consumption/production rate following an Arrhenius law

$$\dot{\omega}_F = -k(\rho/\overline{W})Y_F \exp\left(\frac{-E_a}{R_u T}\right), \tag{17}$$

whose kinetic parameters E_a/R_u and k represent the activation temperature and the pre-exponential factor of the reaction; the subscript F denotes the fuel. These parameters are typically determined from fitting procedures using detailed chemistry as a target to match constant volume delay times over a temperature range of interest and/or ideal ZND profiles; see Taileb et al. [21] and Yuan et al. [27] for details. To specify the mixture using a simplified scheme three additional quantities need being defined: the heat release Q, molecular weight

$\overline{W}$, and γ. For a stoichiometric H_2-O_2 mixture fitted to the detailed mechanism of Mével et al. [28], $E_a/R_u = 14160$ K, $k = 6 \times 10^9$ s^{-1}, $\overline{W} = 12$ g/mol, $\gamma = 1.33$ and $Q = 4.8$ MJ/kg.

2.4.2. 3-step chain-branching chemistry

Chemical reactions usually take place as a sequence of intermediate stages that include chain-initiation, chain-branching and termination steps. This sequence, known to mimic H_2 chemistry well, can be introduced by a slightly more complex model with three reactions; subscripts I, B and C denote, respectively, the initiation, branching and termination steps. The scheme reads:

$$\begin{aligned} \text{Initiation:} \quad & F \text{ (Fuel)} \rightarrow R \text{ (Chain-carriers)}, \\ & r_I = k_I(\rho/\overline{W})Y_F \exp\left(\frac{-E_I}{R_u T}\right), \end{aligned} \tag{18}$$

$$\begin{aligned} \text{Branching:} \quad & F + R \rightarrow 2R, \\ & r_B = k_B(\rho/\overline{W})^2 Y_F Y_R \exp\left(\frac{-E_B}{R_u T}\right), \end{aligned} \tag{19}$$

$$\begin{aligned} \text{Termination:} \quad & R \rightarrow P \text{ (Products)}, \\ & r_C = k_C(\rho/\overline{W})Y_R, \end{aligned} \tag{20}$$

where r_I, r_B and r_C represent the reaction rates, E_I/R_u and E_B/R_u are the activation temperatures, and $k_I = k_C \exp(E_I/R_u T_I)$, $k_B = k_C(W/\rho_{vN}) \exp(E_B/R_u T_B)$ and k_C are the pre-exponential factors; ρ_{vN} is the von Neumann density about which the fitting with detailed chemistry is done. The net production/consumption rates of fuel, F, and chain carriers, R, are $\dot{\omega}_F = -r_I - r_B$ and $\dot{\omega}_R = r_I + r_B - r_C$, respectively. This kind of simplified schemes can be applied to fuels that exhibit a change of slope in induction delay time, τ_{ind}, vs. inverse temperature, $1/T$, semilogarithmic plots such as H_2 (see Fig. 3 (a)) or ethylene [29]. The possibility of including additional physics with a marginal increase in computational cost makes them particularly attractive. The kinetic and mixture parameters for this model

are: $\rho_{vN} = 2.684$ kg/m^3, $E_I/R_u = 25000$ K, $E_B/R_u = 8500$ K, $T_I = 2431$ K, $T_B = 1350$ K, $k_c = 2 \times 10^7$ s^{-1}, $\overline{W} = 12$ g/mol, $\gamma = 1.33$ and $Q = 4.99$ MJ/kg. These were determined following the same methodology described in the previous subsection.

2.4.3. Detailed chemistry

Different detailed mechanisms have been developed over the years to reproduce H_2 oxidation. They are complex, include numerous intermediate steps, and provide the best available modeling for this fuel. The added complexity brings about an increase in computational cost, as more species need being included and, therefore, the number of equations to be solved becomes larger.

The chemical mechanism of Mével et al. [28] is used as our reference to compare against the simplified kinetic schemes described above. It includes 9 species and 21 reactions and has been widely validated against experimental measurements of ignition delay times, flame speed, detonation speeds and cell sizes, and has shown good predictive capabilities in detonation quenching [21] and transmission [30] studies. Three additional detailed mechanisms, Ó Conaire et al. [31], San Diego [32] and GRI 3.0 [33], are used to assess differences in their $c_{f,\text{crit}}$ predictions. Every single one of the detailed mechanism includes pressure-dependent reaction rates and are widely used in the combustion community. Finally, all the chemical mechanisms, including those for simplified kinetics, were implemented using *.cti* files (included as supplementary material).

3. Numerical integration and root-finding algorithm

The numerical integration of the system of ODEs was performed using the SDT algorithm as a base. The following changes were made in the *ZND_system* class: (i) the momentum equation was included; not required in the ideal case as the induction zone velocity is constant and determined via the shock jump conditions alone. (ii) the right hand side (RHS) of the equations were modified to include the functions F_q and F. Note that the default integration

method used in the *solve ivp* function of the *Scipy* package [34], was also changed from *Radau* (implicit Runge-Kutta) to *BDF* (Backward Differentiation Formula). A very robust stiff solver is needed because the RHS of the system can become very large as one approaches the sonic point (which is itself a critical point of the system of ODEs).

In contrast to the ideal steady solutions found with the ZND model, detonations with friction losses admit two (or more) steady solutions for a particular value of c_f. The solution methodolody, irrespective of whether we are dealing with ideal or non-ideal cases, consists of marching downstream from the postshock state until the flow Mach number relative to the leading shock is unity, $M = \mathrm{w}/a_f = 1$. For this to occur the numerator and denominator of the RHS should vanish simultaneously; these are referred to as removable discontinuities or singularities of the 0/0 type. At large velocity deficits, $D/D_{CJ} \leq 0.56$, a sonic point is not attained and a steady solution is reached when the flow comes to rest in the laboratory frame. The numerical procedure used to obtain the aforementioned solutions follows. For a given value of the shock velocity, D, the system of ODEs is integrated varying c_f, until the optimum value is found, $c_{f,\mathrm{opt}}$. Once the integration is finished, we can discern if the solution is valid by checking the spatial distribution of the Mach number downstream of the leading shock as follows:

- *Solution with a sonic point* (Fig. 2(a)-left). If $c_f < c_{f,\mathrm{opt}}$ (blue line), the Mach number reaches unity with an increasing slope that approaches infinity, related to the presence of a strong singularity in the flow. If $c_f > c_{f,\mathrm{opt}}$ (red line), the loss term is too strong and the flow does not reach sonicity. The sought for solution, $c_f = c_{f,\mathrm{opt}}$, is obtained when $M = 1$ is approached with a slowly varying slope (green line).

- *Solution without a sonic point* (Fig. 2(b)-left). The first possible outcome is the same as that described above for $c_f < c_{f,\mathrm{opt}}$ (blue line). If $c_f > c_{f,\mathrm{opt}}$, the Mach number will progressively decrease and drop abruptly after chemical reactions take place (red

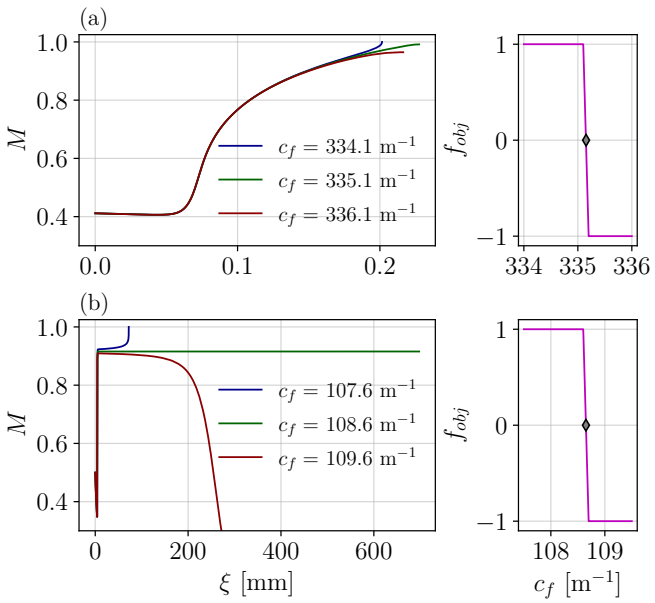

Figure 2: *Left.* Flow Mach number spatial distribution obtained for a steady detonation moving at (a) $D \approx 0.9 D_{CJ}$ and (b) $D \approx 0.475 D_{CJ}$ for three different friction coefficients, c_f. *Right.* Sign change in objective function, f_{obj}, for varying c_f; the sought for solutions –diamonds– occur when $f_{obj}(c_f) = 0$. Conditions: stoichiometric H_2-O_2 at $p_0 = 100$ kPa and $T_0 = 300$ K. The chemistry was modeled using the mechanism of Mével et al. [28].

line). A trial solution is considered valid if the Mach number remains constant for at least, $\xi \approx 0.5$ m (green line).

For both cases, the solution is found using the same objective function

$$f_{obj} = \frac{M_{max} - (1 - \delta M)}{|M_{max} - (1 - \delta M)|}, \tag{21}$$

with δM a small value on the order of 10^{-4}; reducing δM further did not result in appreciable changes in the $c_{f,\text{opt}}$ values obtained. The objective function, f_{obj}, was derived based on the work of Klein et al. for detonations with curvature losses [35]. We found useful and straight-forward to use the Mach number profile to define our convergence metric. The validity of a pair (D, c_f) is verified by looking at the $M(\xi)$ profile around the sonic point or where the flow velocity in the laboratory frame, u, approaches zero. For a given D, if $c_f < c_{f,\text{opt}}$, M_{max} is always unity and the numerator of f_{obj} is always positive. By scaling

it by its absolute value, $f_{obj} = 1$. If $c_f > c_{f,\mathrm{opt}}$, $M_{max} < (1 - \delta M)$ yielding a negative the numerator and $f_{obj} = -1$. $f_{obj}\, vs.\, c_f$ is shown in Fig. 2-right for two representative cases: (a) $D \approx 0.9 D_{CJ}$ and (b) $D \approx 0.475 D_{CJ}$, both computed with the detailed mechanism of Mével et al. [28]. The desired value of c_f occurs when $f_{obj}(c_f) = 0$ obtained by recursively dividing an initial closed interval $[c_{f,\mathrm{min}}, c_{f,\mathrm{max}}]$ bracketing a sign change of the objective function with a tolerance around 10^{-5}; that is, the root of f_{obj} is found using the bisection method. In Semenko et al. [11] an alternative way of finding the steady solutions was presented. The authors suggested a change of variables that effectively removes the singularity in the governing equations. While it does not seem straight-forward to extend their formulation to more general cases with temperature dependent thermodynamics and/or complex chemistry we used their work and results to validate our implementation; see Appendix B for details.

4. Results and discussion

An extensive analysis of the quasi-steady one-dimensional solutions for stoichiometric H_2-O_2 detonations with friction losses was performed. For all the results shown below the thermodynamic conditions ahead of the shock (fresh gases) were kept constant at $p_0 =$ 100 kPa and $T_0 = 300$ K, respectively.

4.1. $D - c_f$ curves

4.1.1. Simplified kinetics vs. detailed chemistry

Figure 3 (a) shows the $D - c_f$ curves obtained with one-step, three-step chain-branching kinetics and detailed chemistry. Relevant detonation and thermodynamic properties predicted by the simplified and detailed mechanisms used in the present study are given in table 1. The results speak for themselves. There are significant differences between simplified schemes that were designed to reproduce the constant volume delay times of detailed chemistry (Fig. 3 (b)), yielding very different detonation velocities for a given friction coefficient,

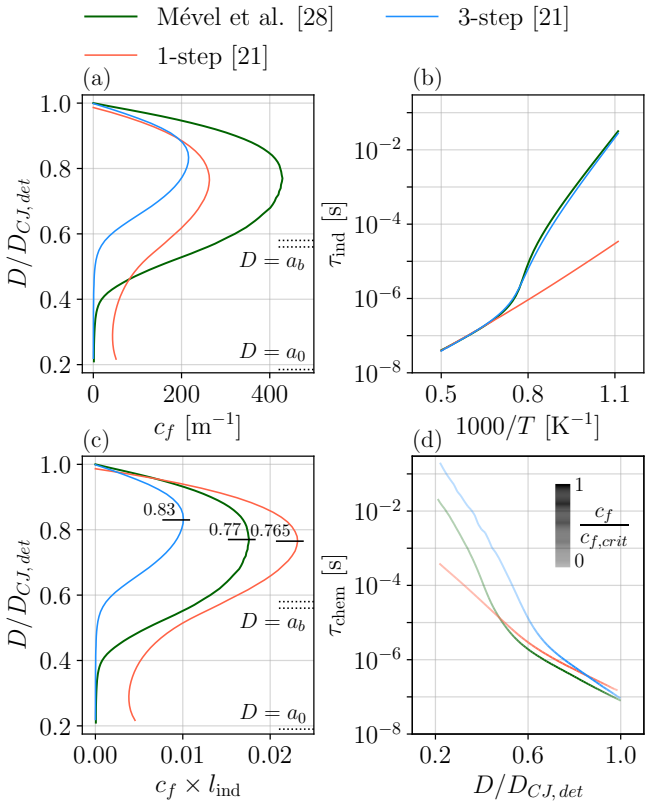

Figure 3: (a) $D - c_f$ curves, (b) τ_{ind}, induction times at constant volume (ρ_{vN}) for stoichiometric H_2-O_2 at $p_0 = 100$ kPa and $T_0 = 300$ K. The range of temperature and pressure considered are $900\,\text{K} < T < 2000\,\text{K}$ and $1.67\,\text{MPa} < p < 3.72\,\text{MPa}$, (c) $D - c_f$ curves scaled with the ideal induction length and (d) integrated chemical times, τ_{chem}, obtained with the single-step and three-step chain-branching kinetics [21] and the detailed mechanism of Mével et al. [28]. The horizontal dotted lines denote the limits –upper/lower bounds obtained with simplified/detailed kinetics– for the quasi-detonation ($a_b \leq D \leq D_{CJ}$) and choking ($a_0 \leq D \leq a_b$) regimes. The $D/D_{CJ,det}$ value at which the first turning point occurs for each mechanism is included in (c). The intensity change of the lines in (d) represent the scaled friction coefficient, $c_f/c_{f,\text{crit}}$, for a given value of $D/D_{CJ,det}$.

Table 1: Detonation properties predicted for a stoichiometric H_2-O_2 mixture with different simplified kinetic schemes and the detailed mechanism of Mével et al. [28]. Initial conditions of the reactive mixture: $p_0 = 100$ kPa and $T_0 = 300$ K.

	D_{CJ} [m/s]	T_{vN} [K]	p_{vN} [MPa]	γ (0 - vN - CJ)	l_{ind} [μm]	$\overline{E}/R_uT_0$
Mével et al. [28]	2839.9	1768.7	3.29	1.4 - 1.315 - 1.218	41.0	27.5
1-step [21]	2801.5	1674.8	3.25	1.33	87.9	34.5
New 1-step	2836.9	1769.5	3.31	1.35	57.7	34.0
3-step [21]	2850.4	1723.7	3.37	1.33	46.8	30.5
New 3-step	2836.2	1768.7	3.30	1.35	25.2	30.1

c_f. The differences are both qualitative (1-step vs. 3-step/det. chem.) and quantitative (1-step/3-step vs. det. chem.), and do not seem to be simply scaled by the ZND induction length (Fig. 3 (c)), l_{ind}, defined as the distance from the leading shock to the peak in thermicity, $\dot{\sigma}$. This makes it difficult to perform a meaningful comparison of the peculiarities of each model. Similar observations regarding the inadequacy of simplified kinetic schemes to qualitatively and quantitatively reproduce the outcomes obtained with detailed chemistry were also discussed by Liberman et al. [36] but in the context of detonation initiation by temperature gradients. At this point, we just provide an overview of the possible reasons behind the found discrepancies.

Before discussing the $D - c_f$ curves further, it is instructive to go over the most salient findings of previous studies. Zeldovich et al. [5] analyzed the eigenvalue problem posed above in the limit of strong heat release. The authors restricted their investigation to relatively high D values close to the curve's first turning point ($D > a_b$; $a_b = 0.58D_{CJ,\,det}$ with the simplified mechanisms and $a_b = 0.56D_{CJ,\,det}$ with detailed mechanisms). Brailovsky and Sivashinsky [6] extended the solutions in [5] after realizing the possibility of having an entirely subsonic flow field behind the detonation wave; their $D - c_f$ curves showed the emergence of a second turning point within the velocity interval $0.185D_{CJ,\,det} = a_0 < D < a_b$ where subscripts 0 and b refer to fresh and burnt gases, respectively. This outcome suggested the existence of an additional *stable* detonation regime including planar as well as galloping and spinning

waves [6]. The c_f values associated to the special points described are denoted $c_{f,0}$ and $c_{f,b}$. For $c_f > c_{f,0}$ the wave does not quench but propagates shockless (sustained by drag-induced diffusion of pressure and adiabatic compression); the gas flow is subsonic throughout the entire structure. The latter solution referred to as *subsonic detonations* [6, 37, 38] were not pursued in the present study. Figure 3 (a) thus includes the *quasi-detonation* and *choking* regimes bounded by $a_b \leq D \leq D_{CJ}$ and $a_0 \leq D \leq a_b$, respectively. The $D - c_f$ curve for detailed chemistry shows only the existence of one turning point, $c_{f,\text{crit}} = 429$ m^{-1} at $D/D_{CJ,\,det} \approx 0.77$ beyond which no possible steady solutions are found. For $c_f < c_{f,\text{crit}}$ two (or more) steady solutions are possible at low and high $D/D_{CJ,\,det}$ values. At $D/D_{CJ,\,det} < 0.4$ the curve asymptotically reaches $c_f \to 0$ m^{-1} as $D \to 0$ m/s.

One-step Arrhenius kinetics, being it the most common choice of chemical model in similar studies, fails to reproduce the $c_{f,\text{crit}}$ value predicted by detailed chemistry, underestimating it by 39%. Moreover, it exhibits a second turning point at low velocities that leads to the Z-shaped curve, usually reported in the literature; see Brailovsky and Sivashinsky [6] for a detailed discussion. The qualitative difference with the curve obtained with detailed chemistry suggests a potential inadequacy of one-step kinetics to reproduce the expected behavior of stoichiometric H_2-O_2 non-ideal detonations, particularly in the *choking* regime where the chemical times are very likely being under-predicted. Additionally, the absence of an induction length results in an evenly distributed heat release (see $\dot{\sigma}$ profiles in Figs. 6 and 7) in contrast to the abrupt and thin profile predicted with detailed chemistry. In [6] it was shown that the second turning point is less pronounced as the effective reduced activation energy, $\overline{E}/R_u T_0$, increases or may be fully suppressed in the strong heat release limit thereby ruling out the existence of *subsonic detonations*.

While 3-step chain-branching chemistry shows a similar qualitative behavior to that of detailed chemistry, as some of the shortcomings described above are partially addressed, differences are still present. Similarly to one-step kinetics, the normalized detonation velocity

($D/D_{CJ,\,det}$) initially decreases at a faster rate, and $c_{f,\mathrm{crit}}$ is underpredicted compared to detailed chemistry. $D(c_{f,\mathrm{crit}})$ is also 8% higher, and the asymptotic approach to $c_f = 0$ m^{-1} occurs at a higher D value than the detailed chemistry predictions. The latter behavior may be due to the fact that the 3-step scheme does not include a pathway to replenish the radical pool for $T < T_B$, shown to be important in H_2 detonation chemistry [39], and/or assuming a termination step with a null activation energy. We emphasize that fundamental improvements to the simplified schemes are outside of the scope of this work and we restrict our analysis to reporting the differences present among the chemical modeling typically used in detonation research when applied to the study of non-ideal detonations.

Both simplified models assume a constant molecular weight, $\overline{W}$, and ratio of specific heats, γ, which for a stoichiometric H_2-O_2 mixture undergo strong changes across the detonation structure. $\overline{W}$ varies from 12 g/mol to 18 g/mol as the products are mostly water vapor (H_2O); γ goes from $\gamma_0 = 1.4$ in fresh gases to $\gamma_{vN} = 1.31$ at the vN-state, further decreasing to $\gamma_{CJ} = 1.21$ at the CJ-state. All these thermodynamic changes are neglected by the two simplified models considered and may be responsible for some of the discrepancies observed. Again, the fitting of these models in Taileb et al. [21] were performed by matching the detailed chemistry induction times at constant volume (ρ_{vN}) and spanning a temperature range of interest, despite providing acceptable results at ideal conditions, as shown in this section, this fitting procedure does not seem to be appropriate to capture the locus of steady solutions when losses are included (i.e., friction and/or curvature). Fig. 3-(d) shows the chemical reaction times, τ_{chem}, obtained from the integration system (11)–(15) plotted as a function of $D/D_{CJ,\,det}$ (following the $D - c_f$ curve). τ_{chem} defined as the time required for a fluid parcel to travel from the leading shock to the location where $\dot{\sigma}_{\mathrm{max}}$ occurs, accounts for the actual thermodynamic changes in the reaction zone therefore is a more representative reaction metric of the process. The significant differences observed in τ_{chem} for the kinetics considered, provide clues about the qualitative and quantitative differences described above

for the $D - c_f$ curves.

Seeking to improve the predictive capabilities of simplified kinetic schemes for non-ideal detonations, and to enable a meaningful comparison among the chemical modeling techniques tested we introduce an alternative approach in the next section.

4.1.2. Modified simplified kinetics vs. detailed chemistry

Taking the $D-c_f$ curve obtained with detailed chemistry as a target we slightly modified both simplified kinetic schemes. We kept a constant $\overline{W}$ and γ, the same activation and cross-over temperatures (E_a/R_u, E_I/R_u, E_B/R_u, T_I and T_B) as those defined previously, but modified γ (always within the bounds of the real mixture), the total heat release, Q, and the pre-exponential factors, k and k_C, as follows: (i) vary γ and Q simultaneously to find a combination that reproduces T_{vN} and D_{CJ} as best as possible; (ii) check whether the given combination provides reasonable values for $D(c_{f,\text{crit}})$; (iii) Modify k (one-step) and k_C (three-step) until their respective $c_{f,\text{crit}}$ approaches the value predicted by detailed chemistry within an arbitrarily prescribed tolerance; increasing/decreasing k or k_C shifts the curves right/left.

The methodology described above yields the following parameters: $E_a/R_u = 14160$ K, $k = 6.735 \times 10^9$ s^{-1}, $\gamma = 1.35$ and $Q = 4.606$ MJ/kg for one-step; $\rho_{vN} = 2.684$ kg/m^3, $E_I/R_u = 25000$ K, $E_B/R_u = 8500$ K, $T_I = 2431$ K, $T_B = 1350$ K, $k_C = 3.35 \times 10^7$ s^{-1}, $\gamma = 1.35$ and $Q = 4.613$ MJ/kg for three-step chain-branching kinetics. We include in table 1 the ideal detonation properties obtained with the modified chemical schemes. Figure 4 shows the same plots as in Fig. 3 but using the updated simplified schemes. The $D-c_f$ curves are, as expected, in much better agreement with the detailed mechanism but a few differences persist (see Fig. 4-(a)). For 1-step kinetics, the second turning point is still present but captures rather well all the *quasi-detonation* regime. For 3-step chain-branching chemistry despite the additional physics included that results in the correct qualitative behavior (captures the change in activation energy at low temperatures) its quantitative performance is subpar.

The initial decay from $D = D_{CJ}$ to $D = D(c_{f,\text{crit}})$ occurs at a lower rate and $D \leq D(c_{f,\text{crit}})$ is appreciably overestimated. As mentioned above, more fundamental refinements are thus required to improve the predictive capabilities of this scheme. In addition, relaxing the constant $\overline{W}$ and γ assumption, modifying the activation energies of both the initiation and branching steps to better fit the slopes in the τ_{chem} plot, introducing a crossover temperature for the termination step, separating the reaction rates for each step or releasing partial heat during branching –when dealing with hydrocarbons– may be worth examining. The updated constant volume induction times, shown in Fig. 4-(b), do not match those of the detailed mechanism, providing further evidence that this fitting procedure is not representative of the reaction times and thermodynamic changes that take place when dealing scenarios with losses. While the updated mechanisms provide improved τ_{chem} (Fig. 4-(d)) the scaling with l_{ind} continues to provide unsatisfactory results (Fig. 4-(d)).

Note that there exists a close relationship between τ_{chem} and the $D - c_f$ curves predicted with the different kinetic schemes. Closer inspection of Figs. 4-(a) and (d) shows that for a given $D/D_{CJ,\,det}$, whenever τ_{chem} computed with the simplified models is longer than the detailed, the corresponding c_f is lower.

4.1.3. Detailed chemistry induced uncertainties

Table 2 includes ideal detonation properties obtained with the detailed mechanisms listed in subsection 2.4.3. The thermodynamics among the mechanisms seem to be in good agreement, showing maximum deviations of around 0.2% for D_{CJ}, the vN-state or γ, whereas kinetic related properties such as l_{ind} and $\overline{E}/R_u T_0$, have maximum deviations of 25% and 19%, respectively. The $D - c_f$ curves are shown in Fig. 5-(a). While their qualitative behavior is expectedly similar, the quantitative differences found among the mechanism are rather surprising. Particularly, in their $c_{f,\text{crit}}$ predictions yielding values that range from 247 m^{-1} (GRI 3.0 mechanism [33]) to 429 m^{-1} (Mével et al. [28]), i.e., a 42% increase. There are also minor differences in $D(c_{f,\text{crit}})$, only on the order of a few percent (2.6%), between GRI

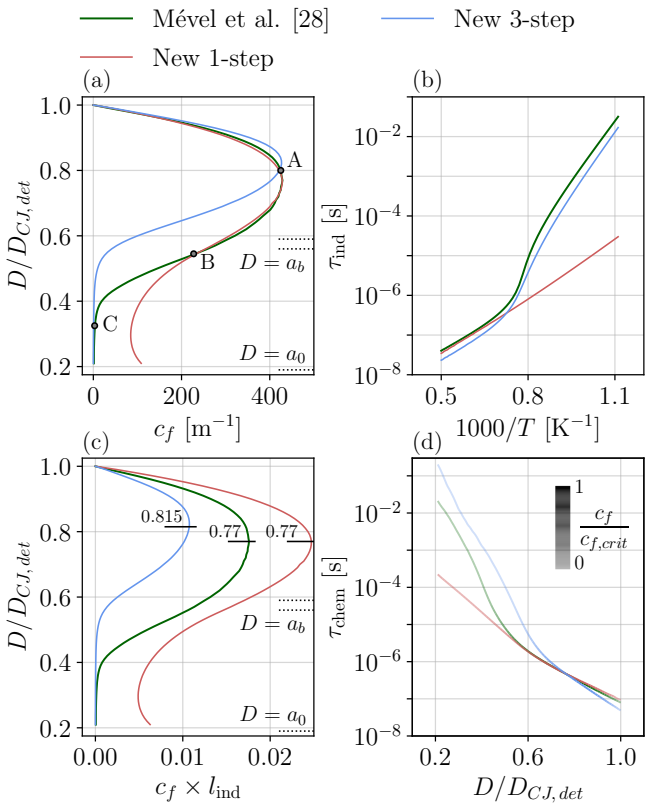

Figure 4: (a) $D - c_f$ curves, (b) induction times at constant volume, τ_{ind}, (c) $D - c_f$ curves scaled with the ideal induction length and (d) integrated chemical times, τ_{chem}, obtained with the updated single-step and three-step chain-branching kinetics [21] and the detailed mechanism of Mével et al. [28]. The horizontal dotted lines denote the limits –upper/lower bounds obtained with simplified/detailed kinetics– for the quasi-detonation ($0.59D_{CJ,det} = a_b \leq D \leq D_{CJ}$) and choking ($a_0 \leq D \leq a_b$) regimes. The round markers in (a) indicate the points at which the p, T, M, $\dot{\sigma}$ and Y_k profiles are analyzed. The $D/D_{CJ,det}$ value at which the first turning point occurs for each mechanism is included in (c). The intensity change of the lines in (d) represent the scaled friction coefficient, $c_f/c_{f,\mathrm{crit}}$, for a given value of $D/D_{CJ,det}$.

Table 2: Detonation properties predicted for a stoichiometric H_2-O_2 mixture with different detailed chemistry mechanisms. Initial conditions: $p_0 = 100$ kPa and $T_0 = 300$ K.

	D_{CJ} [m/s]	T_{vN} [K]	p_{vN} [bar]	γ (0 - vN - CJ)	l_{ind} [μm]	$\overline{E}/R_uT_0$
Mével et al. [28]	2839.9	1768.7	32.9	1.4 - 1.315 - 1.218	41.0	27.5
Ó Conaire [31]	2840.0	1768.8	32.9	1.4 - 1.315 - 1.219	41.3	27.4
San Diego [32]	2835.0	1764.1	32.7	1.4 - 1.316 - 1.214	49.7	27.9
GRI 3.0 [33]	2835.7	1764.2	32.8	1.4 - 1.316 - 1.213	51.1	32.6

(0.79) and Mével (0.77). The differences in induction times, τ_{ind}, (Fig. 5-(b)) and chemical times, τ_{chem}, (Fig. 5-(d)) among the mechanisms may partly explain the dissimilar $c_{f,\text{crit}}$ predictions. Fig. 5-(c) shows an inverse relation between l_{ind} given by the detailed mechanism and the critical friction coefficient $c_{f,\text{crit}}$ (i.e., smaller l_{ind} results in larger $c_{f,\text{crit}}$); a dependence that does not hold for the simplified schemes. To fully understand the reported discrepancies between the detailed mechanisms, which are of the same order of magnitude than those predicted by the original simplified mechanisms used [21], requires a thorough chemical analysis which is outside of the scope of this study.

4.2. Reaction zone structures

p, T, M, $\dot{\sigma}$ and Y_k profiles are computed for values of $D/D_{CJ,\,det}$ and c_f where (some of) the curves coexist (Points A, B and C in Fig. 4-(a)). Note that the axes may vary between different figures for the sake of clarity.

4.2.1. Modified simplified kinetics vs. detailed chemistry

Figure 6 shows the profiles calculated for a detonation in the *quasi-detonation* regime ($D \approx 0.8 D_{CJ,\,det}$) with $c_f \approx 422$ m^{-1} (point A in Fig. 4-(a)). The profiles somewhat resemble the ideal ZND structures except that pressure/temperature increase in the induction zone, and the flow Mach number, M, decreases as result of heating due to friction. The postshock state is $p_s/p_{vN} = 0.63$ and $T_s/T_{vN} = 0.71$. The 3-step chain-branching scheme and the detail mechanism do not react until $\xi \sim 4\, l_{\text{ind det}}$, single-step and its inability to reproduce an induction length results in slow consumption of the mixture immediately after the shock.

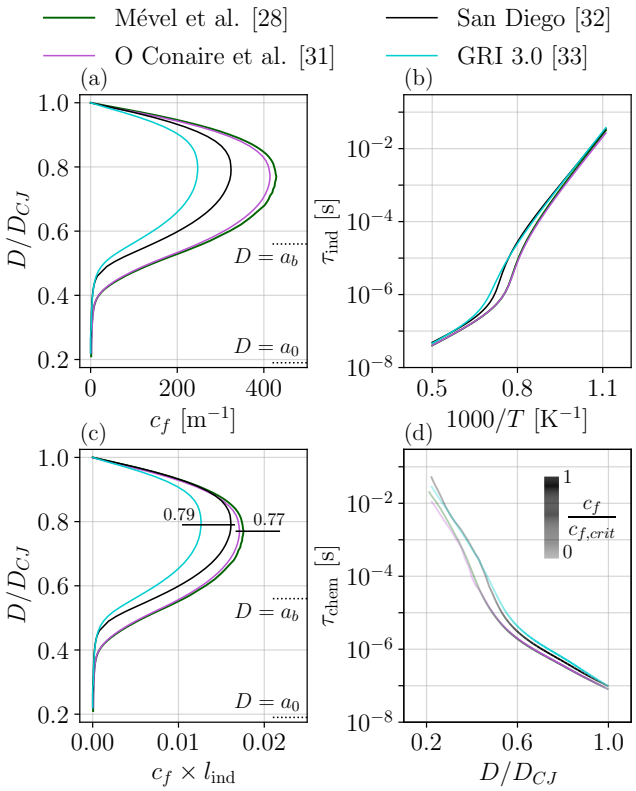

Figure 5: (a) $D-c_f$ curves scaled with their respective D_{CJ}, (b) induction times at constant volume, τ_{ind}, (c) $D-c_f$ curves scaled with the ideal induction length and (d) integrated chemical times, τ_{chem}, obtained with all detailed mechanisms considered. The horizontal dotted lines denote the limits for the quasi-detonation ($a_b \leq D \leq D_{CJ}$) and choking ($a_0 \leq D \leq a_b$) regimes. The D/D_{CJ} value at which the first turning point occurs for each mechanism is included in (c). The intensity change of the lines in (d) represent the scaled friction coefficient, $c_f/c_{f,\mathrm{crit}}$, for a given value of D/D_{CJ}.

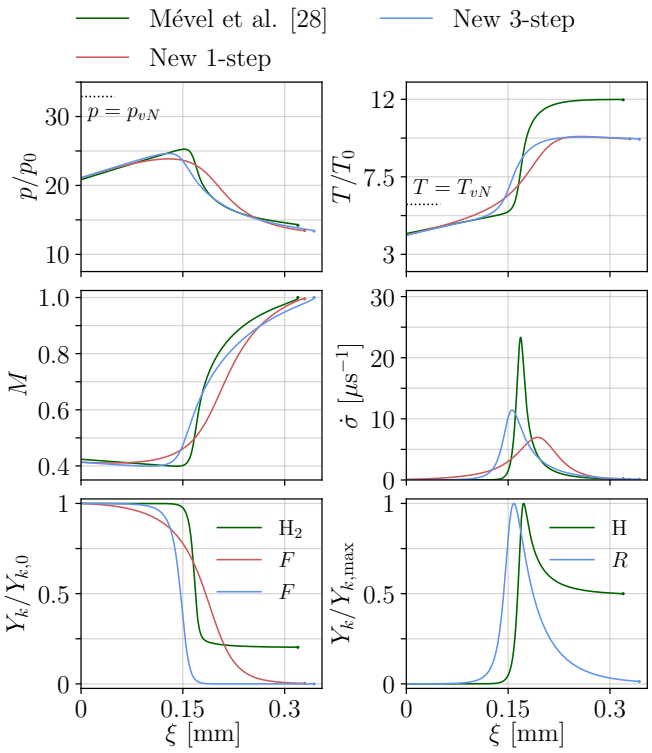

Figure 6: p, T, M, $\dot{\sigma}$ and scaled Y_k profiles obtained for a shock velocity $D = 0.8D_{CJ,\,det}$ and a friction factor of $c_f \approx 422$ m^{-1} with the 1-step, 3-step and the detailed chemical mechanism of Mével et al [28].

Once reactions are fully activated, heat release takes place at a rate given by the shape of the thermicity profiles. The detailed mechanism exhibits the fastest and narrowest profile, whereas the one-step shows an evenly distributed and wider profile. The higher temperature predicted by the detailed mechanism, is due to the variation of the molecular weight $\overline{W}$ and γ as the reaction takes place which in not included in the simplified schemes. Contrary to detailed kinetics, the fuel mass fraction profiles show that the simplified schemes deplete all the available fuel at the end of the reaction zone. Notably, after all the chemical heat is deposited into the flow, all the three mechanisms predict the appearance of a sonic region at distances around $\xi \sim 0.33$ mm behind the shock.

The flow conditions change for larger deficits (point B in Fig. 4-(a)) as we move into the *choking* regime ($D = 0.55D_{CJ,\,det}$ and $c_f = 240$ m^{-1}), where only the curves for 1- step

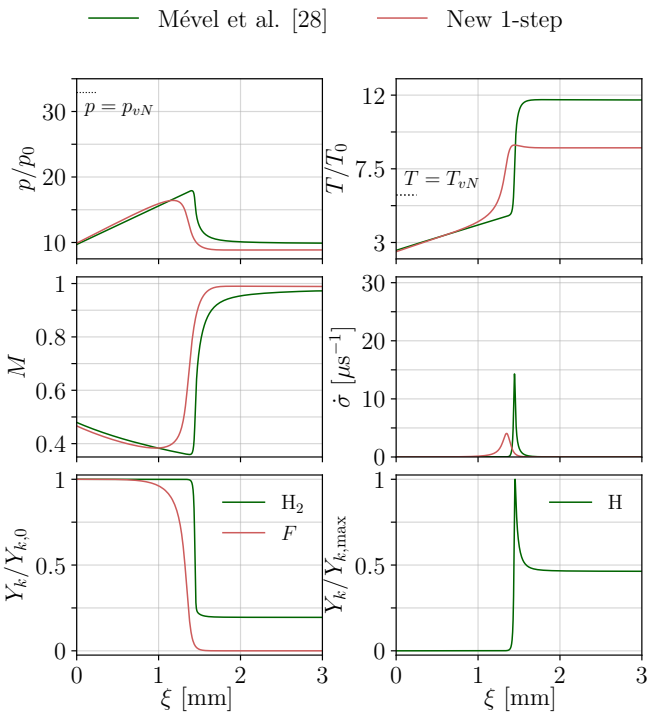

Figure 7: p, T, M, $\dot{\sigma}$ and scaled Y_k profiles obtained for a shock velocity $D = 0.55 D_{CJ,\,det}$) and a friction factor of $c_f = 240$ m^{-1} with the 1-step and the detailed chemical mechanism of Mével et al [28].

and detailed chemistry intersect (Fig. 7). The shock is weak with postshock pressure and temperature of $p_s/p_{vN} = 0.29$ and $T_s/T_{vN} = 0.42$. It is at these conditions when the influence of heating due to friction should be comparable to that of the chemical energy release. The shocked but unreacted mixture heats up at a slow but constant rate, which makes the reaction zone move far downstream, at distances of the order of millimeters ($\xi \sim 40\, l_{\mathrm{ind,\,det}}$). The shorter induction times predicted by the 1-step mechanism result in faster ignition of the mixture (see $\dot{\sigma}$ profiles). In spite of this, the overall reaction zone structure is similar for both chemical models except for a significantly thicker main heat release zone. The mass fraction profiles show these qualitative differences clearly. Note that the flow does not reach sonicity and the boundary condition is satisfied at infinity (not shown here for clarity).

Figure 8 compares the profiles obtained with detailed chemistry and 3-step chain-branching kinetics for $D = 0.325 D_{CJ,\,det}$, close to the speed of sound in the fresh mixture. The general outline is very similar to the one described above, but with significantly lower postshock states ($p_s/p_{vN} = 0.11$ and $T_s/T_{vN} = 0.25$), slower pressure build-up and frictional heating as a result of a $c_f \to 0$ m^{-1}. This leads to a main heat release zone located at distances of around half a meter downstream the shock. The applicability of an inviscid model to adequately capture the reaction zone structure of waves propagating at such large deficits is questionable. It is plausible that if thermal/mass diffusion were to be included in the model the computed structures would differ, however, the fact that *shockless* solutions sustained by drag-induced diffusion of pressure and adiabatic compression were shown to exist in [6] for larger deficits may suggest otherwise.

A quick order of magnitude analysis of the different time/length scales present in our physical system may help substantiate this argument. First, given the slowest computed shock speed (i.e., $D = 0.21 D_{CJ,\,det} \sim 600$ m/s) and an axial characteristic length of $L_x \sim 6$ m (i.e., reaction zone length at these conditions), the convective transient time yields $\tau_{\mathrm{conv}} \sim L_x/D \sim 10$ ms. Second, the characteristic chemical time from the computation of the steady

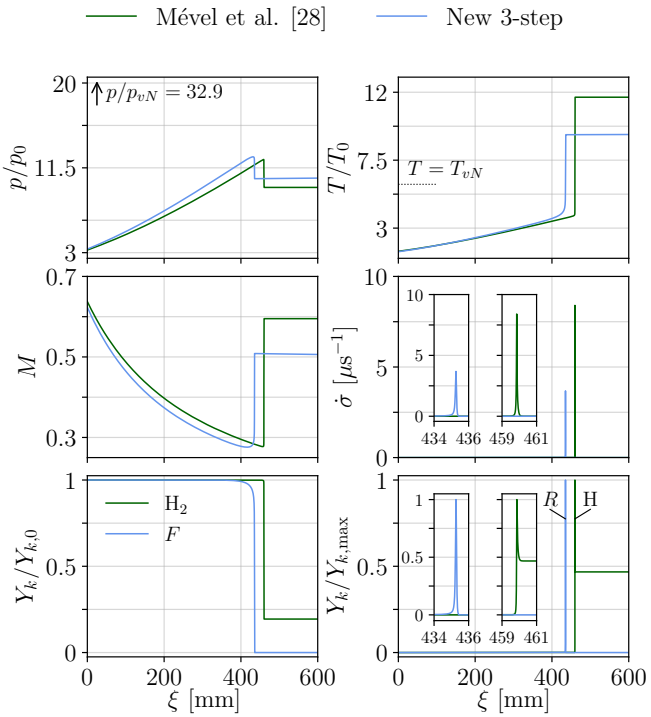

Figure 8: p, T, M, $\dot{\sigma}$ and scaled Y_k profiles obtained for a shock velocity $D = 0.325 D_{CJ,\,det}$) and a friction factor of $c_f = 3.75$ m^{-1} with the 3-step and detailed chemical mechanism of Mével et al [28].

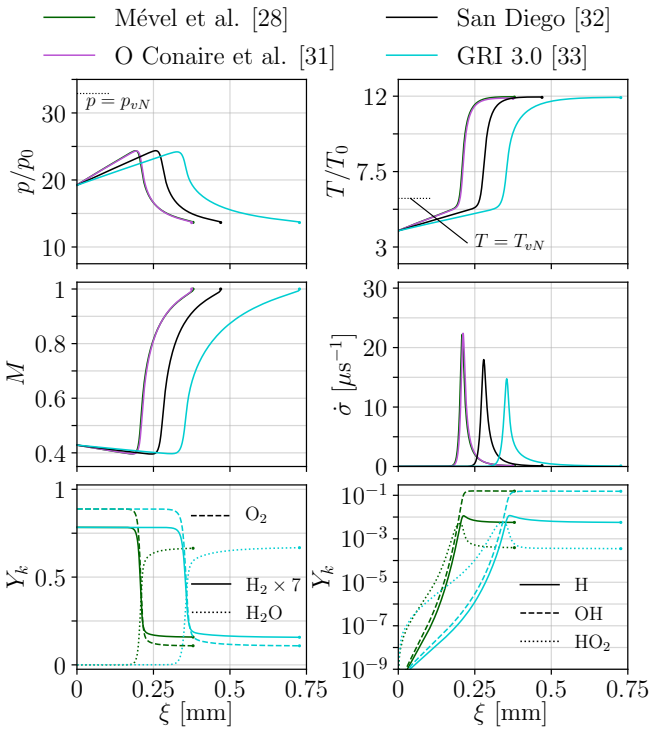

Figure 9: p, T, M, $\dot{\sigma}$ and Y_k profiles obtained for a shock velocity $D = 0.77D_{CJ}$) and its correspondent friction factor of $c_f = c_{f,\text{crit}}$ m^{-1} with the detailed chemical mechanisms. The species are only depicted for Mével et al. [28] and GRI 3.0 [33] for the sake of clarity.

solution is $\tau_{\text{chem}} \sim 20$ ms. The diffusive length scale computed using the thermal diffusivity at postshock conditions ($T_s \sim 320$ K and $P_s \sim 1.3 \times 10^5$ Pa), $\alpha_s \sim 7.7 \times 10^{-5}$ m^2/s, is $L_\alpha \sim \sqrt{\tau_{\text{conv}}\alpha_s} \sim 1$ mm. These results suggest that thermal diffusive proccesses in the wave propagation direction play a minor role, and convective and chemical terms drive the reaction zones at near-sonic conditions. However, radial heat losses may still be important which our one-dimensional model does not account for.

4.2.2. Detailed chemistry induced uncertainties

Figure 9 shows the profiles obtained with all the detailed mechanisms used for $D = 0.77D_{CJ}$ and their corresponding friction factors which are $c_{f,\text{crit}}$ for Mével and O' Conaire, and slightly below for GRI and San Diego. Since all the detailed mechanisms share the same thermodynamic database, the postshock conditions are identical. However, as mentioned

before, there are significant disprepancies in the predicted criticality with $c_{f,\mathrm{crit}}$ ranging from 247 to 429 m^{-1}, which expectedly results in differences in their reaction zone structures. It seems to be mostly a spatial shift and higher rates of pressure/temperature increase for higher c_f values. This results in the thermicity profiles peaking at different locations and attaining different maxima. However, the total amount of energy deposited by the exothermic reaction is approximately the same; how fast/much and the location where chemical heat release occurs in the flow plays a key role on the reaction zone structures.

The way in which the intermediate elementary chemical reactions proceed is important.

The mass fraction profiles show similar behaviors for the consumption of fuel/oxidizer and the production of H_2O. However, differences in the production/consumption of radicals in the reaction zone are evident. First, the net production/consumption rate of both OH and H is fastest when using the mechanism of Mével et al. [28] (only the GRI 3.0 [28] and Mével are plotted for clarity). These differences may be reinforced by the fastest heating rate due to friction for Mével when the pathways that create these radicals are activated (at $\xi \approx 50$ μm). Second, the behavior of HO_2 is peculiar. Just behind the shock, GRI 3.0 favors a higher HO_2 production rate. Soon after, its production rate decreases and Mével et al. overcomes it, resulting in an overall faster chemical times. Note that the behavior described may be an artifact of having the main reaction zones occurring at different locations downstream. However, a preliminary sensitivity analysis on the pre-exponential factors of the elementary reactions ($O + H_2 \leftrightarrow H + OH$ and $H + H_2O_2 \leftrightarrow HO_2 + H_2$) that were found to have the largest differences between GRI and Mével (10 and 6 orders of magnitude, respectively) brings the $c_{f,\mathrm{crit}}$ of GRI to closer to that of Mével. The rates of production/consumption of HO_2 and OH seem to be a key aspect for adequate prediction of the steady reaction zones of detonation with friction losses; the competition for radicals has also been shown to be important in multidimensional detonations [39]. Given the large differences among the detailed mechanisms tested, including the mechanism induced uncertainties to the critical

diameter estimates such as those reported in [22–24] will certainly give a more fair assessment of the predictive capabilities of the model.

5. Conclusions

We revisited the problem of one-dimensional steady detonations with friction losses and analyzed the influence of the chemistry modeling making use of both simplified (one-step and three-step chain-branching) and detailed kinetics. First, we compared the results obtained with simplified schemes, fitted using conventional methods such as matching the constant volume ignition delay times, to those of detailed mechanisms commonly used in the literature for hydrogen oxidation. Both simplified schemes failed to capture the critical c_f values predicted with detailed kinetics. While the three-step chain-branching successfully reproduced the qualitative trend of the reference $D - c_f$ curve, the one-step scheme showed qualitative differences in the *choking* regime likely due to the under-prediction of the H_2-O_2 ignition delay times at postshock temperatures below the chain-branching cross-over temperature. Second, an alternative approach to fit simplified schemes was introduced aiming to reproduce the $D - c_f$ curves obtained with a reference detailed mechanism. The resulting modified schemes were expectedly capable of better reproducing the reaction zones of detonations with friction losses. In particular, the 1-step mechanism was found to be in agreement for the entire *quasi-detonation* regime whereas the *choking* regime continued to be over predicted (i.e., larger c_f values for a fixed velocity deficit D/D_{CJ}). The 3-step mechanism retains its good qualitative agreement but predicts lower deficits at fixed c_f in the latter regime. Suggestions to improve the predictive capabilities of the simplified schemes were proposed. Additionally, the detailed mechanism induced uncertainties in the prediction of $c_{f,\mathrm{crit}}$ were quantified. We found differences of up to 42% between the lowest (GRI) and highest (Mével et al.) $c_{f,\mathrm{crit}}$ predicted; this difference is somewhat reconciled by scaling the curves using their respective ideal induction lengths, l_{ind}. We identified the importance of

the consumption/creation rates of the HO_2 radical pool in the postshock region as a potential culprit for the discrepancies observed; a more in-depth analysis will nonetheless be required to verify this.

Future efforts will be directed to further understand: (i) the transition between low and high velocity solutions at a fixed c_f with a transient solver and (ii) the influence of heat losses on the reaction zone structures of detonations with friction losses, both, using detailed kinetics; comparisons with available experimental data will be possible with this model. Determining transient $D - c_f$ curves and characterizing their behaviors close to failure may also be an avenue worth exploring.

6. Acknowledgements

The authors want to acknowledge the financial support from the Agence Nationale de la Recherche Program JCJC (FASTD ANR-20-CE05-0011-01).

References

[1] I. Jain, Hydrogen the fuel for 21st century, Int. J. Hydrogen Energ. 34 (2009) 7368–7378.

[2] A. M. Abdalla, S. Hossain, O. B. Nisfindy, A. T. Azad, M. Dawood, A. K. Azad, Hydrogen production, storage, transportation and key challenges with applications: a review, Energ. Convers. Manage. 165 (2018) 602–627.

[3] G. Ciccarelli, S. Dorofeev, Flame acceleration and transition to detonation in ducts, Prog. Energ. Combust. 34 (2008) 499–550.

[4] J. E. Shepherd, Detonation in gases, Proc. Combust. Inst. 32 (2009) 83–98.

[5] Y. B. Zel'dovich, B. Gel'Fand, Y. M. Kazhdan, S. Frolov, Detonation propagation in a rough tube taking account of deceleration and heat transfer, Combust. Explo. Shock+ 23 (1987) 342–349.

[6] I. Brailovskya, G. Sivashinsky, Hydraulic resistance and multiplicity of detonation regimes, Combust. Flame 122 (2000) 130–138.

[7] P. Gordon, S. Kamin, G. Sivashinsky, On initiation of subsonic detonation in porous media combustion, Asymptotic Anal. 29 (2002) 309–321.

[8] V. Tanguay, A. Higgins, On the inclusion of frictional work in non-ideal detonations, 20th ICDERS meeting (2005) paper 228.

[9] R. Semenko, A. Kasimov, One-dimensional modeling of gaseous detonation in a packed bed of solid spheres, 24th ICDERS meeting (2013) paper 68.

[10] L. M. Faria, A. R. Kasimov, Qualitative modeling of the dynamics of detonations with losses, Proc. Combust. Inst. 35 (2015) 2015–2023.

[11] R. Semenko, L. Faria, A. R. Kasimov, B. Ermolaev, Set-valued solutions for non-ideal detonation, Shock Waves 26 (2016) 141–160.

[12] A. Sow, A. Chinnayya, A. Hadjadj, Mean structure of one-dimensional unstable detonations with friction, J. Fluid Mech. 743 (2014) 503–533.

[13] A. Higgins, Steady one-dimensional detonations, in: F. Zhang (Ed.), Shock Waves Science and Technology Library, Vol. 6, Springer, Heidelberg, 2012, pp. 33–105.

[14] I. Brailovsky, G. I. Sivashinsky, Momentum loss as a mechanism for deflagration-to-detonation transition, Combust. Theor. Model. 2 (1998) 429–447.

[15] I. Brailovsky, G. I. Sivashinsky, Hydraulic resistance as a mechanism for deflagration-to-detonation transition, Combust. Flame 122 (2000) 492–499.

[16] A. R. Kasimov, D. S. Stewart, On the dynamics of self-sustained one-dimensional detonations: A numerical study in the shock-attached frame, Phys. Fluids 16 (2004) 3566–3578.

[17] A. Sow, A. Chinnayya, A. Hadjadj, Effect of friction and heat losses on the mean structure of one-dimensional detonations, AIP Conf. Proc. 1558 (2013) 140–143.

[18] A. Sow, A. Kasimov, On the dynamics of one-dimensional gaseous detonations with losses, in: Progress in Detonation Physics, Torus Press, Moscow, 2016, pp. 148–149.

[19] M. Reynaud, F. Virot, A. Chinnayya, A computational study of the interaction of gaseous detonations with a compressible layer, Phys. Fluids 29 (2017) 056101.

[20] A. Sow, A. Chinnayya, A. Hadjadj, On the viscous boundary layer of weakly unstable detonations in narrow channels, Comput. Fluids 179 (2019) 449–458.

[21] S. Taileb, J. Melguizo-Gavilanes, A. Chinnayya, Influence of the chemical modeling on the quenching limits of gaseous detonation waves confined by an inert layer, Combust. Flame 218 (2020) 247–259.

[22] G. Agafonov, S. Frolov, Computation of the detonation limits in gaseous hydrogen-containing mixtures, Combust. Explo. Shock+ 30 (1994) 91–100.

[23] S. Kitano, M. Fukao, A. Susa, N. Tsuboi, A. Hayashi, M. Koshi, Spinning detonation and velocity

deficit in small diameter tubes, Proc. Combust. Inst. 32 (2009) 2355–2362.

[24] N. Tsuboi, Y. Morii, A. K. Hayashi, Two-dimensional numerical simulation on galloping detonation in a narrow channel, Proc. Combust. Inst. 34 (2013) 1999–2007.

[25] S. Browne, J. Ziegler, J. Shepherd, Numerical solution methods for shock and detonation jump conditions, Report No. FM2006, Caltech Aerospace (GALCIT), Pasadena, CA, USA, 2008.

[26] D. G. Goodwin, R. L. Speth, H. K. Moffat, B. W. Weber, Cantera: An object-oriented software toolkit for chemical kinetics, thermodynamics, and transport processes, `https://www.cantera.org`, version 2.5.1 (2021). doi:10.5281/zenodo.4527812.

[27] X. Yuan, C. Yan, J. Zhou, H. Ng, Computational study of gaseous cellular detonation diffraction and re-initiation by small obstacle induced perturbations, Phys. of Fluids 33 (2021) 047115.

[28] R. Mével, J. Sabard, J. Lei, N. Chaumeix, Fundamental combustion properties of oxygen enriched hydrogen/air mixtures relevant to safety analysis: Experimental and simulation study, Int. J. Hydrogen Energ. 41 (2016) 6905–6916.

[29] R. Mével, J. Melguizo-Gavilanes, L. Boeck, J. Shepherd, Hot surface ignition of ethylene-air mixtures: Selection of reaction models for cfd simulations, 10th U.S. National Combustion Meeting (2017) paper 2RK–0098.

[30] J. Melguizo-Gavilanes, V. Rodriguez, P. Vidal, R. Zitoun, Dynamics of detonation transmission and propagation in a curved chamber: a numerical and experimental analysis, Combust. Flame 223 (2021) 460–473.

[31] M. Ó Conaire, H. J. Curran, J. M. Simmie, W. J. Pitz, C. K. Westbrook, A comprehensive modeling study of hydrogen oxidation, Int. J. Chem. Kinet. 36 (2004) 603–622.

[32] Chemical-kinetic mechanisms for combustion applications, `https://web.eng.ucsd.edu/mae/groups/combustion/mechanism.html`.

[33] G. P. Smith, D. M. Golden, M. Frenklach, N. W. Moriarty, B. Eiteneer, M. Goldenberg, C. T. Bowman, R. K. Hanson, S. Song, W. C. Gardiner, V. V. L. Jr., Z. Qin, Gri 3.0 chemical mechanism, `http://www.me.berkeley.edu/gri-mech/`.

[34] P. Virtanen, R. Gommers, T. E. Oliphant, M. Haberland, T. Reddy, D. Cournapeau, E. Burovski, P. Peterson, W. Weckesser, J. Bright, S. J. van der Walt, M. Brett, J. Wilson, K. J. Millman, N. Mayorov, A. R. J. Nelson, E. Jones, R. Kern, E. Larson, C. J. Carey, İ. Polat, Y. Feng, E. W. Moore, J. VanderPlas, D. Laxalde, J. Perktold, R. Cimrman, I. Henriksen, E. A. Quintero, C. R. Harris, A. M. Archibald, A. H. Ribeiro, F. Pedregosa, P. van Mulbregt, SciPy 1.0 Contributors, SciPy 1.0:

Fundamental Algorithms for Scientific Computing in Python, Nature Methods 17 (2020) 261–272. doi:10.1038/s41592-019-0686-2.

[35] R. Klein, J. Krok, J. Shepherd, Curved quasi-steady detonations: Asymptotic analysis and detailed chemical kinetics, Report No. FM 95-04, Caltech Aerospace (GALCIT), Pasadena, CA, USA, 1995.

[36] Liberman, Michael and Wang, Cheng and Qian, Chengeng and Liu, JianNan, Influence of chemical kinetics on spontaneous waves and detonation initiation in highly reactive and low reactive mixtures, Combust. Theor. Model. 23 (2019) 467–495.

[37] I. Brailovsky, V. Goldshtein, I. Shreiber, G. Sivashinsky, On combustion waves driven by diffusion of pressure, Combust. Sci. Technol. 124 (1997) 145–165.

[38] I. Brailovsky, G. I. Sivashinsky, On deflagration-to-detonation transition, Combust. Sci. Technol. 130 (1997) 201–231.

[39] Z. Liang, S. Browne, R. Deiterding, J. Shepherd, Detonation front structure and the competition for radicals, Proc. Combust. Inst. 31 (2007) 2445–2453.

Appendix A. Detailed formulation algebra

Appendix A.1. Thermicity form

Starting from Eqs. (1)-(4) and for convenience in subsequent derivation, the energy equation (3) can be explicitly expressed in terms of the specific enthalpy, h, and entropy, s, of the mixture. Recalling the themodynamic identity $\mathrm{d}h = T\mathrm{d}s + 1/\rho\ \mathrm{d}p + \sum_{k=1}^{N} g_k \mathrm{d}Y_k$, where g_k is the specific Gibbs free energy of species k and T is the gas temperature, the changes denoted by $\mathrm{d}h$, $\mathrm{d}s$, etc. are those taking place within a given fluid parcel, and can be written using the material derivative, D/Dt. In these variables the energy equation reads:

$$\rho \frac{Dh}{Dt} - \frac{Dp}{Dt} = uf, \tag{A.1}$$

$$\frac{Ds}{Dt} = \frac{1}{T}\left[\frac{uf}{\rho} - \sum_{k=1}^{N} g_k \frac{DY_k}{Dt}\right], \tag{A.2}$$

For gaseous reacting mixtures pressure is a function of the density, the specific entropy and the species mass fractions $p(\rho, s, \mathbf{Y})$, with $\mathbf{Y}$ representing a vector that includes all species k. Expanding yields:

$$\frac{Dp}{Dt} = \left.\frac{\partial p}{\partial \rho}\right|_{s,\mathbf{Y}} \frac{D\rho}{Dt} + \left.\frac{\partial p}{\partial s}\right|_{\rho,\mathbf{Y}} \frac{Ds}{Dt} + \sum_{k=1}^{N} \left.\frac{\partial p}{\partial Y_k}\right|_{\rho,s,Y_{i\neq k}} \frac{DY_k}{Dt}. \tag{A.3}$$

Replacing the expression for Ds/Dt (Eq. (A.2)),

$$\begin{aligned}\frac{Dp}{Dt} = \left.\frac{\partial p}{\partial \rho}\right|_{s,\mathbf{Y}} \frac{D\rho}{Dt} + \left.\frac{\partial p}{\partial s}\right|_{\rho,\mathbf{Y}} \left[\frac{1}{T}\left(\frac{uf}{\rho} - \sum_{k=1}^{N} g_k \frac{DY_k}{Dt}\right)\right] + \\ + \sum_{k=1}^{N} \left.\frac{\partial p}{\partial Y_k}\right|_{\rho,s,Y_{i\neq k}} \frac{DY_k}{Dt}.\end{aligned} \tag{A.4}$$

Rearranging,

$$\frac{Dp}{Dt} = \left.\frac{\partial p}{\partial \rho}\right|_{s,\mathbf{Y}} \frac{D\rho}{Dt} + \left.\frac{\partial p}{\partial s}\right|_{\rho,\mathbf{Y}} \left[\frac{1}{T}\left(\frac{uf}{\rho}\right)\right] + \\ + \sum_{k=1}^{N} \left[-\frac{g_k}{T}\left.\frac{\partial p}{\partial s}\right|_{\rho,\mathbf{Y}} + \left.\frac{\partial p}{\partial Y_k}\right|_{\rho,s,Y_{i\neq k}}\right] \frac{DY_k}{Dt}. \tag{A.5}$$

where $\left.\frac{\partial p}{\partial \rho}\right|_{s,\mathbf{Y}} = a_f^2$ is the frozen sound speed of the mixture. Assuming the mixture to behave as an ideal gas, the second term in the right hand side of Eq. (A.5) simplifies to:

$$\left.\frac{\partial p}{\partial s}\right|_{\rho,\mathbf{Y}} \frac{1}{\rho T} = \frac{1}{\left.\frac{\partial s}{\partial p}\right|_{\rho,\mathbf{Y}}} \frac{1}{\rho T} = \frac{p}{T c_v \rho} = \frac{R_g}{c_v} = \gamma - 1 \\ \text{with } \frac{p}{\rho} = R_g T, \tag{A.6}$$

all symbols in Eq. (A.6) are defined in the main body of the text. Introducing the thermicity, $\dot{\sigma}$, in general form,

$$\dot{\sigma} = \sum_{k=1}^{N} \sigma_k \frac{DY_k}{Dt}, \tag{A.7}$$

where σ_k is given by,

$$\sigma_k = -\frac{g_k}{T}\left.\frac{\partial p}{\partial s}\right|_{\rho,\mathbf{Y}} + \left.\frac{\partial p}{\partial Y_k}\right|_{\rho,s,Y_{i\neq k}}. \tag{A.8}$$

and restricting it to ideal gases, yields:

$$\sigma_k = \frac{\overline{W}}{W_k} - \frac{h_k}{c_p T}. \tag{A.9}$$

Replacing Eq. (A.6) in (A.5) and using definitions (A.7) and (A.9), Eq. (A.5) becomes:

$$\frac{Dp}{Dt} = a_f^2 \frac{D\rho}{Dt} + (\gamma - 1)uf + \rho a_f^2 \dot{\sigma}. \tag{A.10}$$

which replaces the energy equation (3) in the system of equations (5)-(8).

Appendix A.2. Wave-fixed frame of reference

For conciseness, the derivation is continued from Eq. (10) of the main body of the manuscript. Using Eq. (9) in system (5)-(8) yields:

$$\mathrm{w}\frac{\mathrm{d}\rho}{\mathrm{d}\xi} + \rho\frac{\mathrm{dw}}{\mathrm{d}\xi} = 0, \tag{A.11}$$

$$\mathrm{w}\frac{\mathrm{dw}}{\mathrm{d}\xi} + \frac{1}{\rho}\frac{\mathrm{d}p}{\mathrm{d}\xi} = \frac{f}{\rho}, \tag{A.12}$$

$$\mathrm{w}\frac{\mathrm{d}p}{\mathrm{d}\xi} - \mathrm{w}a_f^2\frac{\mathrm{d}\rho}{\mathrm{d}\xi} = (\gamma - 1)uf + \rho a_f^2 \dot{\sigma}, \tag{A.13}$$

$$\mathrm{w}\frac{\mathrm{d}Y_k}{\mathrm{d}\xi} = \frac{W_k \dot{\omega}_k}{\rho}, \quad k = 1, ..., N. \tag{A.14}$$

Restricting the system to seek for steady solutions (i.e., $\partial/\partial t = 0$) the time derivatives vanish, resulting in the mapping below:

$$\frac{D}{Dt} \rightarrow \mathrm{w}\frac{\mathrm{d}}{\mathrm{d}\xi}. \tag{A.15}$$

Combining like terms, rearranging and introducing the variable $\eta = 1 - M^2$ where $M = \mathrm{w}/a_f$, is the frozen flow Mach number gives:

$$\frac{\mathrm{d}\rho}{\mathrm{d}\xi} = -\frac{\rho}{\mathrm{w}}\left[\frac{\dot{\sigma} + F_q - F}{\eta} + F\right], \tag{A.16}$$

$$\frac{\mathrm{dw}}{\mathrm{d}\xi} = \frac{\dot{\sigma} + F_q - F}{\eta} + F, \tag{A.17}$$

$$\frac{\mathrm{d}p}{\mathrm{d}\xi} = -\rho\mathrm{w}\left[\frac{\dot{\sigma} + F_q - F}{\eta}\right], \tag{A.18}$$

$$\mathrm{w}\frac{\mathrm{d}Y_k}{\mathrm{d}\xi} = \frac{W_k\dot{\omega}_k}{\rho}, \quad k = 1, ..., N. \tag{A.19}$$

Finally noting that for a detonation wave propagating at a constant speed $\mathrm{d}/\mathrm{d}t = \mathrm{w}(\mathrm{d}/\mathrm{d}\xi)$, the system of equations given by Eqs. (11)-(16) is recovered.

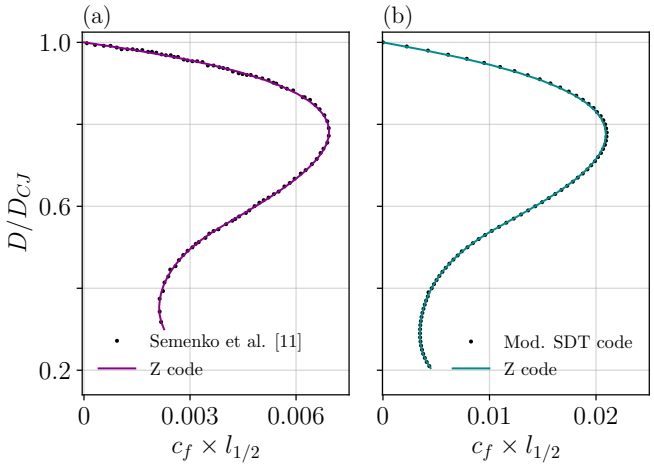

Figure A.10: Comparison of the $D/D_{CJ} - c_f$ curves obtained by (a) Semenko et al. [11] ($\phi = 0.4$, $E = 30$, $Q = 20$ and $\gamma = 1.2$) with an in-house implementation of their framework (Z code); (b) the Z code and the updated SDT algorithm using the 1-step kinetics of Taileb et al. [21] for H_2-O_2 ideal detonations ($\phi = 1$, $\gamma = 1.33$). The x-axes are multiplied by their respective half-reaction lengths, $l_{1/2}$.

Appendix B. Numerical code validation

The validation of the numerical implementation was carried out as follows: First, the algorithm and mathematical techniques of Semenko et al. [11] –named Z code– were im-

plemented and compared against their results (Fig. A.10-(a)). Second, taking the standard SDT code as a base, the friction losses terms were added. $D - c_f$ curves were then computed using the updated SDT algorithm and the Z code for the 1-step mechanism presented in Taileb et al. [21]. The results are shown in Fig. A.10-(b); the agreement is evident.